CLEO CONF 98-07
ICHEP98 849

First Observation Of The Decay $B^0 \to D^{*+}D^{*-}$

CLEO Collaboration

(July 21, 1998)

Abstract

We report on the first observation of the decay $\mathrm{B}^0 \to \mathrm{D}^{*+}\mathrm{D}^{*-}$ with the CLEO detector. In $5.6\,\mathrm{fb}^{-1}$ of $\Upsilon(4S)$ data, four $\mathrm{B}^0 \to \mathrm{D}^{*+}\mathrm{D}^{*-}$ candidates were observed in fully reconstructed decay modes. The background contribution in the signal region is estimated to be less than 0.37 ± 0.11. The probability for the background to fluctuate up to the observed number of events or larger is less than 8.7×10^{-5}. From the observed yield and Monte Carlo simulation of the $\mathrm{B}^0 \to \mathrm{D}^{*+}\mathrm{D}^{*-}$ decay in the CLEO detector, we estimate the branching fraction to be:

$$\mathcal{B}(\mathrm{B}^0 \to \mathrm{D}^{*+}\mathrm{D}^{*-}) = (7.8^{+5.4}_{-3.8} \pm 1.5) \times 10^{-4} \quad .$$

D. E. Jaffe,[1] G. Masek,[1] H. P. Paar,[1] E. M. Potter,[1] S. Prell,[1] V. Sharma,[1] D. M. Asner,[2] J. Gronberg,[2] T. S. Hill,[2] D. J. Lange,[2] R. J. Morrison,[2] T. K. Nelson,[2] D. Roberts,[2] B. H. Behrens,[3] W. T. Ford,[3] A. Gritsan,[3] H. Krieg,[3] J. Roy,[3] J. G. Smith,[3] J. P. Alexander,[4] R. Baker,[4] C. Bebek,[4] B. E. Berger,[4] K. Berkelman,[4] V. Boisvert,[4] D. G. Cassel,[4] D. S. Crowcroft,[4] M. Dickson,[4] S. von Dombrowski,[4] P. S. Drell,[4] K. M. Ecklund,[4] R. Ehrlich,[4] A. D. Foland,[4] P. Gaidarev,[4] R. S. Galik,[4] L. Gibbons,[4] B. Gittelman,[4] S. W. Gray,[4] D. L. Hartill,[4] B. K. Heltsley,[4] P. I. Hopman,[4] J. Kandaswamy,[4] D. L. Kreinick,[4] T. Lee,[4] Y. Liu,[4] N. B. Mistry,[4] C. R. Ng,[4] E. Nordberg,[4] M. Ogg,[4,*] J. R. Patterson,[4] D. Peterson,[4] D. Riley,[4] A. Soffer,[4] B. Valant-Spaight,[4] A. Warburton,[4] C. Ward,[4] M. Athanas,[5] P. Avery,[5] C. D. Jones,[5] M. Lohner,[5] C. Prescott,[5] A. I. Rubiera,[5] J. Yelton,[5] J. Zheng,[5] G. Brandenburg,[6] R. A. Briere,[6] A. Ershov,[6] Y. S. Gao,[6] D. Y.-J. Kim,[6] R. Wilson,[6] H. Yamamoto,[6] T. E. Browder,[7] Y. Li,[7] J. L. Rodriguez,[7] S. K. Sahu,[7] T. Bergfeld,[8] B. I. Eisenstein,[8] J. Ernst,[8] G. E. Gladding,[8] G. D. Gollin,[8] R. M. Hans,[8] E. Johnson,[8] I. Karliner,[8] M. A. Marsh,[8] M. Palmer,[8] M. Selen,[8] J. J. Thaler,[8] K. W. Edwards,[9] A. Bellerive,[10] R. Janicek,[10] P. M. Patel,[10] A. J. Sadoff,[11] R. Ammar,[12] P. Baringer,[12] A. Bean,[12] D. Besson,[12] D. Coppage,[12] C. Darling,[12] R. Davis,[12] S. Kotov,[12] I. Kravchenko,[12] N. Kwak,[12] L. Zhou,[12] S. Anderson,[13] Y. Kubota,[13] S. J. Lee,[13] R. Mahapatra,[13] J. J. O'Neill,[13] R. Poling,[13] T. Riehle,[13] A. Smith,[13] M. S. Alam,[14] S. B. Athar,[14] Z. Ling,[14] A. H. Mahmood,[14] S. Timm,[14] F. Wappler,[14] A. Anastassov,[15] J. E. Duboscq,[15] K. K. Gan,[15] T. Hart,[15] K. Honscheid,[15] H. Kagan,[15] R. Kass,[15] J. Lee,[15] H. Schwarthoff,[15] A. Wolf,[15] M. M. Zoeller,[15] S. J. Richichi,[16] H. Severini,[16] P. Skubic,[16] A. Undrus,[16] M. Bishai,[17] S. Chen,[17] J. Fast,[17] J. W. Hinson,[17] N. Menon,[17] D. H. Miller,[17] E. I. Shibata,[17] I. P. J. Shipsey,[17] S. Glenn,[18] Y. Kwon,[18,†] A.L. Lyon,[18] S. Roberts,[18] E. H. Thorndike,[18] C. P. Jessop,[19] K. Lingel,[19] H. Marsiske,[19] M. L. Perl,[19] V. Savinov,[19] D. Ugolini,[19] X. Zhou,[19] T. E. Coan,[20] V. Fadeyev,[20] I. Korolkov,[20] Y. Maravin,[20] I. Narsky,[20] R. Stroynowski,[20] J. Ye,[20] T. Wlodek,[20] M. Artuso,[21] E. Dambasuren,[21] S. Kopp,[21] G. C. Moneti,[21] R. Mountain,[21] S. Schuh,[21] T. Skwarnicki,[21] S. Stone,[21] A. Titov,[21] G. Viehhauser,[21] J.C. Wang,[21] J. Bartelt,[22] S. E. Csorna,[22] K. W. McLean,[22] S. Marka,[22] Z. Xu,[22] R. Godang,[23] K. Kinoshita,[23] I. C. Lai,[23] P. Pomianowski,[23] S. Schrenk,[23] G. Bonvicini,[24] D. Cinabro,[24] R. Greene,[24] L. P. Perera,[24] G. J. Zhou,[24] S. Chan,[25] G. Eigen,[25] E. Lipeles,[25] J. S. Miller,[25] M. Schmidtler,[25] A. Shapiro,[25] W. M. Sun,[25] J. Urheim,[25] A. J. Weinstein,[25] and F. Würthwein[25]

[1]University of California, San Diego, La Jolla, California 92093
[2]University of California, Santa Barbara, California 93106
[3]University of Colorado, Boulder, Colorado 80309-0390
[4]Cornell University, Ithaca, New York 14853
[5]University of Florida, Gainesville, Florida 32611
[6]Harvard University, Cambridge, Massachusetts 02138

[*]Permanent address: University of Texas, Austin TX 78712.

[†]Permanent address: Yonsei University, Seoul 120-749, Korea.

[7]University of Hawaii at Manoa, Honolulu, Hawaii 96822
[8]University of Illinois, Urbana-Champaign, Illinois 61801
[9]Carleton University, Ottawa, Ontario, Canada K1S 5B6
and the Institute of Particle Physics, Canada
[10]McGill University, Montréal, Québec, Canada H3A 2T8
and the Institute of Particle Physics, Canada
[11]Ithaca College, Ithaca, New York 14850
[12]University of Kansas, Lawrence, Kansas 66045
[13]University of Minnesota, Minneapolis, Minnesota 55455
[14]State University of New York at Albany, Albany, New York 12222
[15]Ohio State University, Columbus, Ohio 43210
[16]University of Oklahoma, Norman, Oklahoma 73019
[17]Purdue University, West Lafayette, Indiana 47907
[18]University of Rochester, Rochester, New York 14627
[19]Stanford Linear Accelerator Center, Stanford University, Stanford, California 94309
[20]Southern Methodist University, Dallas, Texas 75275
[21]Syracuse University, Syracuse, New York 13244
[22]Vanderbilt University, Nashville, Tennessee 37235
[23]Virginia Polytechnic Institute and State University, Blacksburg, Virginia 24061
[24]Wayne State University, Detroit, Michigan 48202
[25]California Institute of Technology, Pasadena, California 91125

I. INTRODUCTION

The Cabbibo-suppressed decay $B^0 \to D^{*+}D^{*-}$ is a promising channel for searches of time-dependent CP-violation in B_d^0 decays. The tree level diagram for the decay $B^0 \to D^{*+}D^{*-}$ is shown in Fig. 1 and is expected to dominate other possible B_d^0 decay mechanisms for producing the same final state. The rate for the process $B^0 \to D^{*+}D^{*-}$ [1] can be estimated

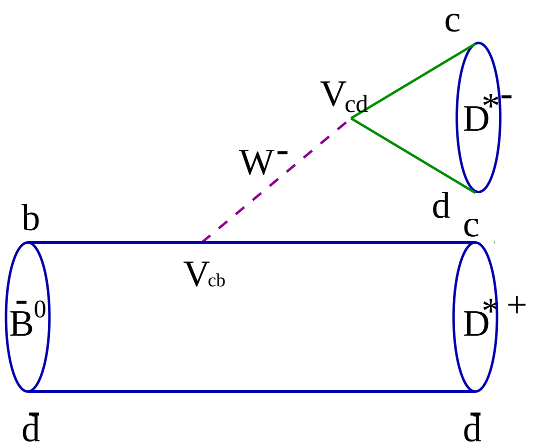

FIG. 1. The Tree level diagram for the process$B^0 \to D^{*+}D^{*-}$.

from the measured rate [1] of the Cabibbo-favoured decay $\overline{B}^0 \to D_s^{*+}D^{*-}$ using the formula

$$\mathcal{B}(B^0 \to D^{*+}D^{*-}) \approx \left(\frac{f_D^*}{f_{D_s^*}}\right)^2 \tan^2\theta_C \mathcal{B}(B^0 \to D_s^{*+}D^{*-}) \tag{1}$$

from which it follows that

$$\mathcal{B}(B^0 \to D^{*+}D^{*-}) \approx 0.1\% \quad . \tag{2}$$

In the past, the CLEO [2] and ALEPH [3] collaborations have searched for this decay mode and have reported upper-limits on the branching fraction. We report on the first observation of the decay $B^0 \to D^{*+}D^{*-}$ and a measurement of its decay rate.

This paper is organized as follows. The CLEO detector, data sample and simulations are described in sec. II. The charm and B_d^0 meson reconstruction is described in sec. III followed by background characterization and estimation in sec. IV. Section V describes our observation and the calculation of the $B^0 \to D^{*+}D^{*-}$ decay rate. We conclude in section VI.

---

[1] Unless explicitly stated, charge-conjugation is implied throughout, and "D" refers to both D^0 and D^+ mesons.

II. DETECTOR AND DATA

The data were recorded with two configurations of the general purpose CLEO detector, called CLEOII and CLEOII.V in this paper.

The CLEO detector in its CLEOII configuration [4] provides charged particle tracking, precision electromagnetic calorimetry, charged particle identification, and muon detection. Charged particle detection over 95% of the solid angle is provided by three concentric wire chambers in a magnetic field of 1.5 T giving a momentum resolution $\sigma_p/p = 0.5\%$ at $p = 1\,\mathrm{GeV}$. The drift chambers are surrounded by a time of flight (TOF) system and a CsI based electromagnetic calorimeter giving an energy resolution $\sigma_E/E = 4\%$ for 100 MeV electromagnetic showers. A superconducting coil and muon detectors surround the calorimeter. Several redundant triggers provided efficient registration of hadronic events. The CLEO detector in its CLEOII.V configuration had its innermost wire chamber replaced by a precision three-layer silicon vertex detector (SVX). Each layer of the SVX is equipped with readout on both sides providing measurements of $r\phi$ and rz coordinates of the charged particles.

The simulation of the CLEO detector response was based upon the GEANT [5] program. Simulated detector response for the CLEOII and CLEOII.V configurations were generated and then processed in the same manner as the data.

The CESR ring operated at a center-of-mass energy of approximately 10.6 GeV. The results in this paper are based upon $3.14\,\mathrm{fb}^{-1}$ of data recorded at the $\Upsilon(4S)$ energy and $1.57\,\mathrm{fb}^{-1}$ 60 MeV lower with the CLEO II detector and $2.46\,\mathrm{fb}^{-1}$ of data at the $\Upsilon(4S)$ energy and $1.26\,\mathrm{fb}^{-1}$ 60 MeV lower with the CLEO II.V detector.

III. $\mathrm{B}^0 \to \mathrm{D}^{*+}\mathrm{D}^{*-}$ CANDIDATE SELECTION

A. D and D^{*+} Reconstruction

Events of the type $\mathrm{B}^0 \to \mathrm{D}^{*+}\mathrm{D}^{*-}$ with the subsequent decays $\mathrm{D}^{*+} \to \mathrm{D}^0\pi^+$ and $\mathrm{D}^{*+} \to \mathrm{D}^+\pi^0$ were selected. The D^0 and D^+ were reconstructed in the eleven different decay modes shown in Table 1. The charged track selection required tracks to originate near the $\mathrm{e}^+\mathrm{e}^-$ interaction point and to have particle identification information from the specific ionization (dE/dx) in the drift chamber and TOF consistent with the D daughter hypotheses of the particular D decay mode. Charged particles and K^0_s from a D candidate were required to originate from a common vertex.

K^0_s were selected through their decay into $\pi^+\pi^-$. The decay point of the K^0_s candidate was required to have a significant displacement from the interaction point. The reconstructed K^0_s candidates was required to originate from the $\mathrm{e}^+\mathrm{e}^-$ interaction point and at least one of the daughter pions was required to be inconsistent with an origin at the interaction point.

Neutral pions were reconstructed from photon pairs detected in the electromagnetic calorimeter. The photons were required to have at least 30 or 50 MeV energy in the barrel or endcap region, respectively, and the invariant mass of each pair was required to be within three standard deviations of the nominal π^0 mass. The π^0 momentum had to be at least 70 and 100 MeV for D^{*+} and D daughters respectively.

TABLE I. D^0 and D^+ decay modes and their product branching fractions [1]. The branching fractions $\mathcal{B}(K^0_s \to \pi^+\pi^-)$ and $\mathcal{B}(\phi \to K^+K^-)$ are included for the modes containing K^0_s or ϕ.

Decay Mode	Branching Ratio (%)
	D^0 Decay Modes
$D^0 \to K^-\pi^+$	3.83 ± 0.12
$D^0 \to K^-\pi^+\pi^0$	13.9 ± 0.9
$D^0 \to K^-\pi^+\pi^+\pi^-$	7.5 ± 0.4
$D^0 \to K^0_s\pi^+\pi^-$	1.8 ± 0.1
$D^0 \to K^0_s\pi^+\pi^-\pi^0$	3.4 ± 0.4
Total D^0 Branching Ratio	30.0
	D^+ Decay Modes
$D^+ \to K^-\pi^+\pi^+$	9.1 ± 0.60
$D^+ \to K^0_s\pi^+$	0.92 ± 0.1
$D^+ \to K^0_s\pi^+\pi^0$	3.24 ± 1.0
$D^+ \to K^0_s\pi^+\pi^+\pi^-$	2.35 ± 0.34
$D^+ \to \phi\pi^+$	0.3 ± 0.03
$D^+ \to \phi\pi^+\pi^0$	1.1 ± 0.5
Total D^+ Branching Ratio	17.1
	D^{*+} Decay Modes
$D^{*+} \to D^0\pi^+_{\rm slow}$	68.3 ± 1.4
$D^{*+} \to D^+\pi^0_{\rm slow}$	30.6 ± 2.5
Total D^{*+} Branching Ratio	99

The D^{*+} candidates were formed from reconstructed D^0 or D^+ candidates by combining them with a charged or neutral pion, respectively. Both $(D^0\pi^+)(\bar{D}^0\pi^-)$ and $(D^0\pi^+)(D^-\pi^0)$ states were reconstructed but not $(D^+\pi^0)(D^-\pi^0)$ as the latter contains two soft neutral pions and therefore engenders prohibitive levels of background. Each D^{*+} candidate was constrained to its nominal mass which improved the D^{*+} momentum resolution by 14% in simulated events.

B. B^0 Reconstruction

$B^0 \to D^{*+}D^{*-}$ candidates were selected by means of four observables. The first observable, $\chi^2_{\rm M}$, is a measure of the deviation of each D or D^{*+} candidate from its nominal mass or mass difference:

$$\chi^2_M \equiv \sum_{i=1,2} \left(\frac{M(D_i) - M_i^{\rm nom}}{\sigma(M_i)}\right)^2 + \left(\frac{\Delta M_i - \Delta M_i^{\rm nom}}{\sigma(\Delta M_i)}\right)^2 \quad . \tag{3}$$

where $\sigma(M_i)$ and $\sigma(\Delta M_i)$ are the average resolutions in $M(D_i)$ and $\Delta M_i = M_i(D^{*+}) - M_i(D)$. If an event has more then one $B^0 \to D^{*+}D^{*-}$ candidate, then the combination with the lowest χ^2_M is chosen.

The second observable, $L/\sigma(L)$, is the significance of the projected three-dimensional distance L between the reconstructed D and $\bar{\mathrm{D}}$ decay vertices. L is defined as

$$L = (\vec{V_{\mathrm{D}}} - \vec{V_{\bar{\mathrm{D}}}}) \cdot \frac{(\vec{P_{\mathrm{D}}} - \vec{P_{\bar{\mathrm{D}}}})}{|\vec{P_{\mathrm{D}}} - \vec{P_{\bar{\mathrm{D}}}}|} \quad .$$

The uncertainty on the distance L, $\sigma(L)$, is calculated from the covariance matrices of the D and $\bar{\mathrm{D}}$ tracks resulting from the vertex fits of the respective D daughters. This variable is effective in the CLEOII.V data for the $(\mathrm{D}^0\pi^+)(\mathrm{D}^-\pi^0)$ candidates because of the relatively long D^+ lifetime and the silicon vertex detector.

The third variable, $\Delta E \equiv E(\mathrm{D}^{*+}) + E(\mathrm{D}^{*-}) - E_{\mathrm{Beam}}$, is a measure of missing energy in the B decay. The resolution in ΔE is 8.0 MeV for $\mathrm{B}^0 \to \mathrm{D}^{*+}\mathrm{D}^{*-}$ events.

The fourth variable is the beam-constrained B mass $M_{\mathrm{B}} \equiv \sqrt{E^2_{\mathrm{Beam}} - \vec{p_{\mathrm{B}}}^2}$. The resolution on M_{B} is 2.5 MeV.

C. Optimization of Observables

To ensure that a signal has the maximum significance, the selection criteria were chosen such that the ratio $S^2/(S+B)$ is maximized. Here S represents the signal, taken from a large sample of simulated events. A branching ratio $\mathcal{B}(\mathrm{B}^0 \to \mathrm{D}^{*+}\mathrm{D}^{*-}) = 10^{-3}$ was used to normalize S. Two independent samples were used to determine the nature of the background and in the optimization of various observables:

1. Simulated events of $\Upsilon(4\mathrm{S}) \to \mathrm{B}\bar{\mathrm{B}}$ with at least one $B \to \mathrm{D}^{*+}X$,
2. "Parity-flip" candidates in data. For a given D candidate we take in turn all low momentum tracks and neutral pions that are not daughters of that D and reverse their 3-momentum. "Parity-flip" $\mathrm{D}^{*+}_{\mathcal{P}}$ candidates are formed from the resulting parity-flipped slow pion candidates and used to create $\mathrm{B}^0 \to \mathrm{D}^{*+}_{\mathcal{P}}\mathrm{D}^{*-}$ which were analyzed as "normal" $\mathrm{B}^0 \to \mathrm{D}^{*+}\mathrm{D}^{*-}$ candidates.

These two background samples have similar distributions in all variables to be optimized. To avoid a bias, these event samples were *not* used in the estimate of the background described in section IV. Using the $S^2/(S+B)$ criterion, the optimal selection criteria are $L/\sigma(L) > 0$ for $(\mathrm{D}^0\pi^+)(\mathrm{D}^-\pi^0)$ candidates in CLEO II.V only, ${\chi^2}_M < 10$, $|\Delta E| < 20$ MeV and $|M_{\mathrm{B}} - M_{\mathrm{B}}^{\mathrm{nom}}| < 6.25$ MeV. In the following, the term "signal region" refers to $|\Delta E| < 20$ MeV and $|M_{\mathrm{B}} - M_{\mathrm{B}}^{\mathrm{nom}}| < 6.25$ MeV.

With these requirements in mind, we discuss the background estimate in the next section.

IV. BACKGROUND ESTIMATES

The background in the reconstruction of $\mathrm{B}^0 \to \mathrm{D}^{*+}\mathrm{D}^{*-}$ can be divided into two categories.

1. Combinatorial background arising from combinations of:

(a) a real D^{*-} and a fake D^{*+},

(b) a fake D^{*-} and a fake D^{*+}.

2. Irreducible backgrounds which arise from pairs of real $D^{*\pm}$ mesons.

   (a) $\Upsilon(4S) \to B\bar{B}$ with $B \to D^{*-}X, \bar{B} \to D^{*+}X$.

   (b) $B \to D^{*-}D^{*+}X_{s,d}$ where $X_{s,d}$ represents either a kaon or other strange meson or a pion, rho or other non-strange meson. These may or may not originate from a D^{**}-like object. These events do not populate the signal region because of the unobserved energy of the particle $X_{s,d}$; however, they may be present in the region outside the signal region.

   (c) $e^+e^- \to c\bar{c}$ with $c \to D^{*+}$ and $\bar{c} \to D^{*-}$.

   Simulations are used to estimate the characteristics of the first two sources of background and data taken 60 MeV below the $\Upsilon(4S)$ are used to estimate the contribution from (c).

A. Estimates of Background Using Data

1. Background Sample 1

The grand side band (GSB) region is defined as the region outside the dotted region in Fig. 2. The boundaries of this region are at $\Delta E = \pm 50$ and ± 400 MeV and at $M_B = 5.26$ GeV. The background estimate in the signal region from the GSB population will be referred to as "Sample 1". The number of events in the GSB region is scaled to the signal region by the ratio of areas $f_{GSB} = (7.3 \pm 2.2) \times 10^{-3}$. The 30 % uncertainty in the scale factor reflects possible deviations from an uniform distribution of the background in ΔE and M_B. The estimated background contribution from Sample 1 to the signal region is 0.26 ± 0.04 events (statistical uncertainty only).

2. Background Sample 2

An independent background estimate can be obtained by considering the sidebands in the D mass plot. This second estimate will be referred to as "Sample 2". For the following discussion, D-background refers to the background at the D mass while D-sideband refers to the two sideband regions in the D mass plot, $\pm 6\sigma(M_i)$, above or below the nominal D mass.

Using these sidebands, two background sub-samples are constructed from the data.

1. A nominal D and a fake $\overline{D}$ formed from the D-sideband where the nominal $\overline{D}$ mass M_i^{nom} in χ^2_M (eqn. 3) is replaced by the value at the center of the upper or lower sideband, $M_i^{nom} \pm 6\sigma(M_i)$. There are two sidebands and two D-candidates so this sample has a weight of 4 compared to the signal sample.

2. A fake D and fake $\overline{\mathrm{D}}$ are formed from the D-sideband by replacing both occurances of M_i^{nom} in χ^2_M with the $M_i^{\mathrm{nom}} \pm 6\sigma(M_i)$. Once again there are four combinations, so this sample has a weight of 4 compared to the signal sample.

These two background sub-samples are subjected to the same selection criteria as the signal sample. The signal sample can be represented as $(R+F)\times(R+F) = R\times R + 2R\times F + F\times F$ with R (F) representing real (fake) D's. The first term represents the number of signal and irreducible background events. The next two terms represent the number of events in categories 1 and 2 of the combinatorial background which can be represented as $B \equiv 4F\times(R+F)$ and $C \equiv 4F\times F$ so that the number of events from the combinatorial background is $B/2 - C/4$. The estimated number of combinatorial background events is scaled to the signal region by the ratio of areas $f_{\mathrm{D}} = (6.9 \pm 2.1)\times 10^{-3}$. This factor is slightly smaller than f_{GSB} as the combinatorial background is determined from the entire $|\Delta E| < 400$ MeV and $5.20 < M_{\mathrm{B}} < 5.29$ GeV region. The estimated combinatorial background contribution from Sample 2 to the signal region is 0.31 ± 0.04 events (statistical uncertainty only).

3. $\mathrm{e^+e^-} \to \mathrm{c\bar{c}} \to \mathrm{D^{*+}D^{*-}}$

The estimate of the irreducible background from the process $\mathrm{e^+e^-} \to c\bar{c}$ with $c \to \mathrm{D^{*+}}$ and $\bar{c} \to \mathrm{D^{*-}}$ is estimated from the data taken at 60 MeV below the $\Upsilon(4\mathrm{S})$ data. Combinatorial background in this data sample is estimated in the same manner and subtracted. The resulting estimate of the number of $c \to \mathrm{D^{*+}}$ and $\bar{c} \to \mathrm{D^{*-}}$ in the signal region is corrected for the relative cross-section and luminosities. It is scaled to the signal region with the scale factor 3.7×10^{-3} which takes into account the expected distribution in ΔE and M_{B} for $c\bar{c}$ production. The estimated $c\bar{c} \to \mathrm{D^{*+}D^{*-}}$ contribution from Sample 2 to the signal region is 0.04 ± 0.03 events (statistical uncertainty only).

B. Estimates of Irreducible Background From Simulations

The inclusive production rate $\mathcal{B}(\mathrm{B} \to \mathrm{D^{*+}}X) = 23.9 \pm 2.0\%$ and the $\mathrm{D^{*+}}$ momentum spectrum have been measured [6]. The process $\Upsilon(4\mathrm{S}) \to \mathrm{B\bar{B}}$, $\mathrm{B} \to \mathrm{D^{*-}}X, \bar{\mathrm{B}} \to \mathrm{D^{*+}}X$ is simulated in the CLEOII and CLEOII.V detector configurations to determine the characteristics of this process. The contribution of this background process to the signal region is estimated to be 0.01 ± 0.01 events (statistical uncertainty only).

Similarly the process $\mathrm{B} \to \mathrm{D^{*-}D^{*+}}X_{\mathrm{s}}$ is simulated and its contribution is determined to be negligible in the ΔE vs M_{B} distribution. The contribution of the process $\mathrm{B} \to \mathrm{D^{*-}D^{*+}}X_{\mathrm{d}}$ is estimated from a simulation of $\mathrm{B} \to \mathrm{D^{*-}}$ "$\mathrm{D^{**+}}$" where "$\mathrm{D^{**}}$" has a mass of 2420 MeV and a width of 400 MeV and is forced to decay to $\mathrm{D^{*+}}\pi^0$. The estimated efficiency for the $\mathrm{D^{*+}}$ and $\mathrm{D^{*-}}$ to be reconstructed with $5.20 < M(\mathrm{B}) < 5.29$ GeV and $|\Delta E| < 400$ MeV is approximately twelve times smaller than the reconstruction efficiency for the signal process, thus we estimate that the contribution from $\mathrm{B} \to \mathrm{D^{*-}D^{*+}}X_{\mathrm{d}}$ is negligible. In addition, because of the energy carried by the unobserved $X_{\mathrm{s,d}}$, candidates from this source will not be reconstructed near the signal region.

V. RESULTS

The distribution in the $\Delta E, M_{\mathrm{B}}$ plane of candidates passing all cuts in the data taken on the $\Upsilon(4S)$ resonance are shown in Figure 2. There are four candidates in the signal region. The projection onto the M_{B} axis when $|\Delta E| < 20$ MeV is shown in figure 3 for the candidates in the data taken on the $\Upsilon(4S)$ resonance.

The distribution in $\Delta E, M_{\mathrm{B}}$ of candidates passing all cuts in the data taken at 60 MeV below the $\Upsilon(4S)$ resonance are shown in Figure 4. Table II lists the D decay mode combi-

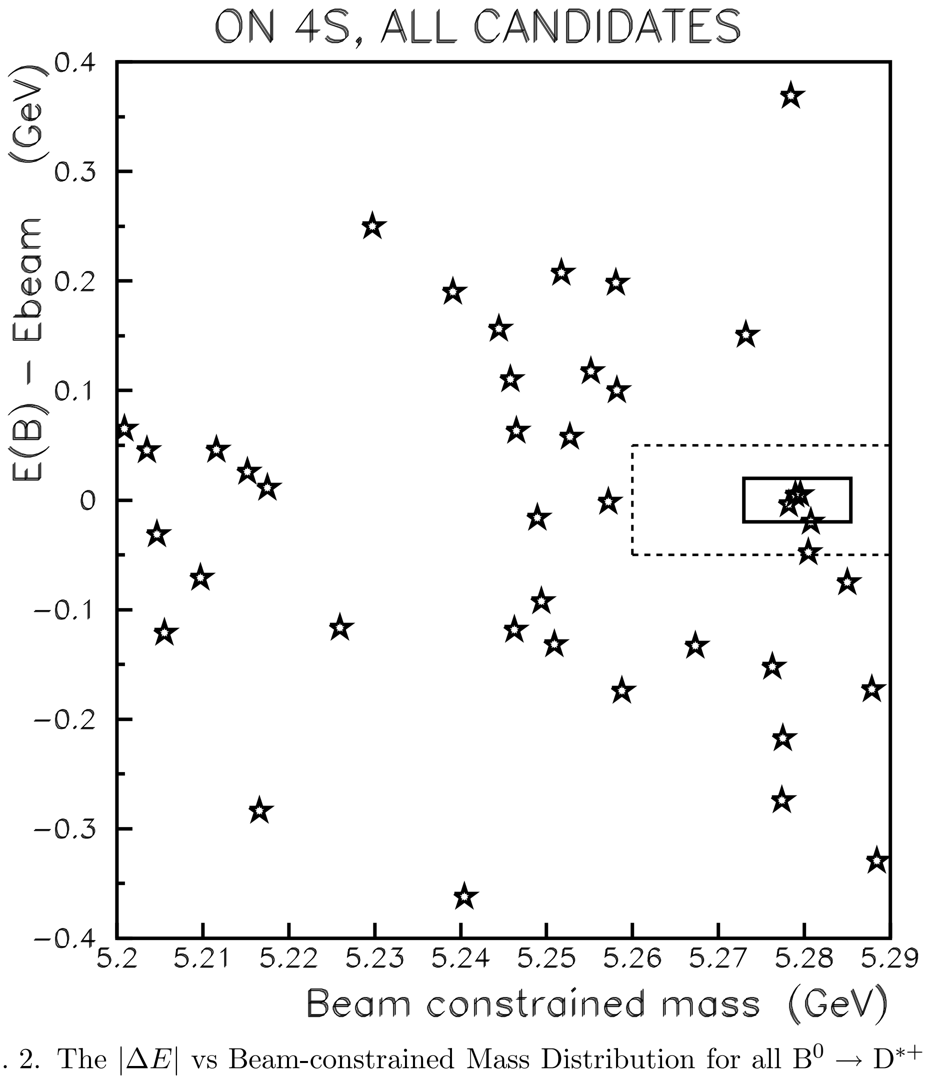

FIG. 2. The $|\Delta E|$ vs Beam-constrained Mass Distribution for all $\mathrm{B}^0 \to \mathrm{D}^{*+}\mathrm{D}^{*-}$ modes in the data taken on the $\Upsilon(4S)$ resonance. The "signal region" is indicated by the box with the solid line. The area outside the dashed line is the grand sideband (GSB).

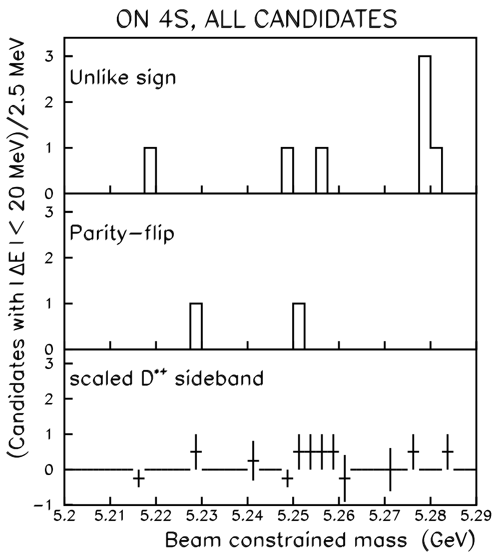

FIG. 3. The Beam-constrained Mass Distribution for all $\overline{\mathrm{B}}^0 \to \mathrm{D}^{*+}\mathrm{D}^{*-}$ modes in the $\Upsilon(4\mathrm{S})$ data after the $|\Delta E| < 20$ MeV cut. The distributions of the "parity-flip" data and the combinatorial background estimated from the D mass sidebands are also shown.

nation for the four $\mathrm{B}^0 \to \mathrm{D}^{*+}\mathrm{D}^{*-}$ candidates observed in the $\Upsilon(4\mathrm{S})$ data which survive all requirements.

TABLE II. The D decay modes of the $\mathrm{B}^0 \to \mathrm{D}^{*+}\mathrm{D}^{*-}$ candidates in the signal region.

D^{*+} mode	D^{*-} mode
$\mathrm{D}^0 \to \mathrm{K}^-\pi^+\pi^0$	$\mathrm{D}^- \to \mathrm{K}^0_s\pi^-$
$\mathrm{D}^0 \to \mathrm{K}^-\pi^+\pi^-\pi^+$	$\bar{\mathrm{D}}^0 \to \mathrm{K}^+\pi^-\pi^-\pi^+$
$\mathrm{D}^0 \to \mathrm{K}^0_s\pi^-\pi^+$	$\bar{\mathrm{D}}^0 \to \mathrm{K}^+\pi^-$
$\mathrm{D}^0 \to \mathrm{K}^0_s\pi^-\pi^+$	$\mathrm{D}^- \to \mathrm{K}^+\pi - \pi^-$

The decay rate for $\overline{\mathrm{B}}^0 \to \mathrm{D}^{*+}\mathrm{D}^{*-}$ is calculated using a likelihood procedure which takes into account the large number of D decay modes and datasets with different sensitivities. The likelihood equation for the branching fraction $\mathcal{B} \equiv \mathcal{B}(\mathrm{B}^0 \to \mathrm{D}^{*+}\mathrm{D}^{*+})$ is

$$\mathcal{L}(\mathcal{B}) = \prod_{i,j,k} \frac{e^{-\mu_{ijk}}\mu_{ijk}^{N_{ijk}}}{N_{ijk}!}$$

where

- i, j, k denotes the D^{*+}, D^{*-} decay modes, and detector configuration (CLEOII or CLEOII.V) respectively.

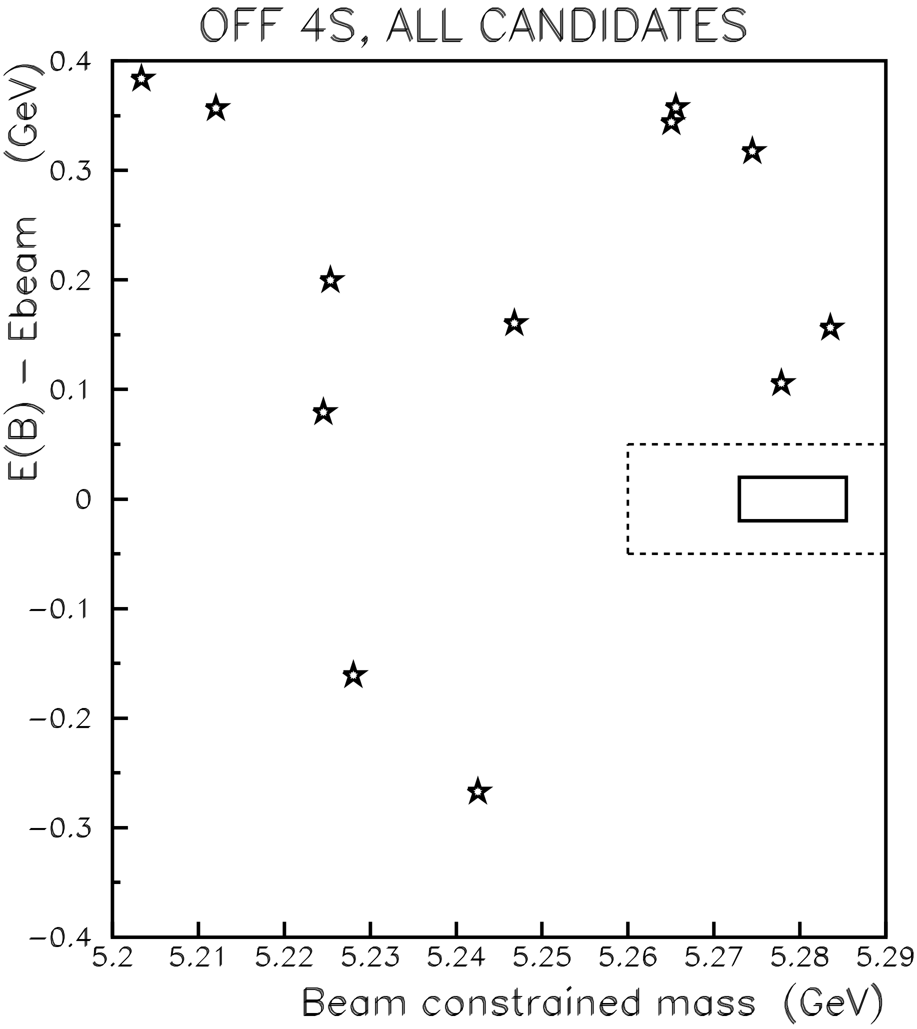

FIG. 4. The $|\Delta E|$ vs Beam-constrained Mass Distribution for all $B^0 \to D^{*+}D^{*-}$ modes for the data take 60 MeV below $\Upsilon(4S)$ resonance.

- N_{ijk} is the observed number of signal candidates,
- $\mu_{ijk} = b_{ijk} + s_{ijk}$ is the expected total number of events,
- b_{ijk} is the estimated number of background events, and
- $s_{ijk} = 2f_{00}N_k(\mathrm{B\bar{B}})\epsilon_{ijk}(\mathrm{D}^{*+},\mathrm{D}^{*-})\mathcal{B}(\mathrm{D}_i^{*+})\mathcal{B}(\mathrm{D}_j^{*-})\mathcal{B}(\mathrm{B}^0 \to \mathrm{D}^{*+}\mathrm{D}^{*-})$ is the expected number of signal events given
  - $\epsilon_{ijk}(\mathrm{D}^{*+},\mathrm{D}^{*-})$ the reconstruction efficiency,
  - $\mathcal{B}(\mathrm{D}_i^{*+})$ the product branching ratio for decay mode i,
  - $N_k(\mathrm{B\bar{B}})$ the number of $\mathrm{B\bar{B}}$ events in dataset k, and
  - $f_{00} = 0.47 \pm 0.04 =$ the fraction of $\Upsilon(4\mathrm{S})$ decays to $\mathrm{B_d^0}\overline{\mathrm{B_d^0}}$ [7].

The reconstruction efficiency, $\epsilon_{ijk}(\mathrm{D}^{*+},\mathrm{D}^{*-})$, of $\mathrm{B}^0 \to \mathrm{D}^{*+}\mathrm{D}^{*-}$ is determined from dedicated signal Monte Carlo generated with the CLEOII and CLEOII.V configuration with approximately 75000 events per configuration. The overall reconstruction efficiency in each data set is shown in Table III. The single event sensitivity SES $\equiv [\epsilon\mathcal{B}N(\mathrm{B_d^0\bar{B}_d^0})]^{-1}$ is estimated from the calculated efficiencies and $N(\mathrm{B_d^0}\overline{\mathrm{B_d^0}})$ to be $(2.3 \pm 0.4) \times 10^{-4}$

TABLE III. Net $\mathrm{B}^0 \to \mathrm{D}^{*+}\mathrm{D}^{*-}$ reconstruction efficiency times branching fractions.

	CLEO2	CLEO2.5	weighted sum
$\epsilon\mathcal{B} \times 10^4$	9.63 ± 1.61	4.71 ± 0.76	7.47 ± 0.96
$N(\mathrm{B_d^0\bar{B}_d^0})$	3.3×10^6	2.5×10^6	5.8×10^6

As a practical matter, there are 90 allowed combinations of modes and datasets, so the estimated number of background events for many i, j, k combinations can be zero given the limited number of events available with either method described above. While it is perfectly reasonable that the estimated background in a particular i, j, k is negligible, the branching fraction $\mathcal{B}$ is calculated with a more inclusive grouping defined as all pairs of modes proceeding via a $(\mathrm{D}^0\pi^+)(\bar{\mathrm{D}}^0\pi^-)$ or $(\mathrm{D}^0\pi^+)(\mathrm{D}^-\pi^0)$ in each detector configuration which reduces $\mathcal{L}(\mathcal{B})$ to a product of four terms.

The expected number of background events in each of the four groups is estimated from the two independent samples described in section IV and shown in Table IV. There is good agreement between the background estimates obtained from the two samples.

In Table IV, the probability that the four candidates are consistent with a fluctuation of the central values of the estimated background rates for the two samples is in the range 3.4 to 7.0×10^{-5}. Including the $\pm 30\%$ relative systematic uncertainty on the scale factors

TABLE IV. The observed number of candidates and estimated background by $D^0\overline{D^0}$ or D^0D^- in each dataset. The row labeled "Total" for Sample 1 is the number of candidates observed in the grand sideband. The rows labeled "Combinatorial background", "$B\bar{B}$ Irreducible background", and "$c\bar{c}$ Irreducible background" for Sample 2 are estimates of the contents of the $5.20 < M(B) < 5.29$ GeV and $|\Delta E| < 400$ MeV region. $\mathbf{P}$(fluctuation) is the probability that the estimated background fluctuates to the number of signal candidates or more in each grouping. The rightmost column contains the product of $\mathbf{P}$(fluctuation). Only statistical uncertainties are included.

	CLEO2		CLEO2.5		Total or
	$D^0\overline{D^0}$	D^0D^-	$D^0\overline{D^0}$	D^0D^-	Product
Signal candidates					
$D^{*+}D^{*-}$ Total	12	27	1	1	41
$D^{*+}D^{*-}$ Signal Region	2	2	0	0	4
Background Sample 1 : Grand Sideband					
Total	10 ± 3.16	24 ± 4.90	1 ± 1	1 ± 1	36 ± 6
Signal region contribution	0.073 ± 0.023	0.174 ± 0.036	0.007 ± 0.007	0.007 ± 0.007	$\mathbf{0.26 \pm 0.04}$
$\mathbf{P}$(fluctuation)	2.5×10^{-3}	1.4×10^{-2}	1	1	3.4×10^{-5}
Background Sample 2 : D mass sidebands					
Combinatorial background	9.75 ± 2.70	32.5 ± 5.02	-0.25 ± 0.66	1.75 ± 1.20	43.75 ± 5.86
$B\bar{B}$ Irreducible background	0.50 ± 0.51	1.00 ± 0.73	0.48 ± 0.49	0.00 ± 0.48	1.98 ± 1.12
$c\bar{c}$ Irreducible background	1.45 ± 3.24	2.90 ± 5.98	1.45 ± 2.22	4.83 ± 3.67	10.6 ± 7.9
Signal region contribution	0.076 ± 0.022	0.243 ± 0.041	0.007 ± 0.010	0.030 ± 0.016	$\mathbf{0.37 \pm 0.05}$
$\mathbf{P}$(fluctuation)	2.8×10^{-3}	2.5×10^{-2}	1	1	7.0×10^{-5}

(f_{GSB} or f_{D}) [2] in quadrature, the probability that the four candidate events are consistent with a background fluctuation is 4.4×10^{-5} (8.7×10^{-5}) for Sample 1 (2).

There are 41 events in the region $5.20 < M(\mathrm{B}) < 5.29$ GeV and $|\Delta E| < 400$ MeV of which 4 candidate events are in the signal region. Using the likelihood method described above, the branching ratio is

$$\mathcal{B}(\mathrm{B}^0 \to \mathrm{D}^{*+}\mathrm{D}^{*-}) = (8.02^{+5.39}_{-3.84} \pm 1.57) \times 10^{-4}$$

and

$$\mathcal{B}(\mathrm{B}^0 \to \mathrm{D}^{*+}\mathrm{D}^{*-}) = (7.66^{+5.37}_{-3.80} \pm 1.50) \times 10^{-4}$$

with the background estimate from Sample 1 and 2, respectively. The first uncertainty is statistical and the second is systematic. The contributions to the systematic uncertainty are 16.6% from the reconstruction efficiency, 8.5% from f_{00}, 5.0% from the number of $\mathrm{B\bar{B}}$ events, and 3.1% from the background parametrization.

The consistency of the decay modes and distribution between the CLEOII and CLEOII.V detector configurations is assessed using the measured ϵ_{ijk} and $N_k(\mathrm{B\bar{B}})$ given the measured branching fraction. The value of $\ln \mathcal{L}(\mathcal{B})$ is calculated for all possible combinations of D^{*+} and D^{*-} decay modes and the two detector configurations and plotted in Figure 5. The value of $\ln \mathcal{L}(\mathcal{B})$ obtained for the four signal candidates is shown as arrow in Figure 5 and demonstrates that the collection of decay modes contributing to the signal candidates listed in Table II is probable.

VI. CONCLUSIONS

We have found 4 candidates for the decay $\mathrm{B}^0 \to \mathrm{D}^{*+}\mathrm{D}^{*-}$ in a sample of 5.8×10^6 $\Upsilon(4S) \to \mathrm{B\bar{B}}$ decays with an estimated background of less than 0.37 ± 0.11 events. The branching fraction is measured to be $\mathcal{B}(\mathrm{B}^0 \to \mathrm{D}^{*+}\mathrm{D}^{*-}) = (7.8^{+5.4}_{-3.8} \pm 1.5) \times 10^{-4}$ in good agreement with the estimate derived from the Cabibbo-allowed decay confirming that this reaction provides an avenue for the measurement of $\sin 2\beta$ at future b-factories. The probability that the estimated background could fluctuate to 4 or more signal events is less than 8.7×10^{-5}.

ACKNOWLEDGMENTS

We gratefully acknowledge the effort of the CESR staff in providing us with excellent luminosity and running conditions. J.R. Patterson and I.P.J. Shipsey thank the NYI program of the NSF, M. Selen thanks the PFF program of the NSF, M. Selen and H. Yamamoto thank the OJI program of DOE, J.R. Patterson, K. Honscheid, M. Selen and V. Sharma thank the A.P. Sloan Foundation, M. Selen and V. Sharma thank the Research Corporation, S. von Dombrowski thanks the Swiss National Science Foundation, and H. Schwarthoff thanks the Alexander von Humboldt Stiftung for support. This work was supported by the

[2] Described in section IV.

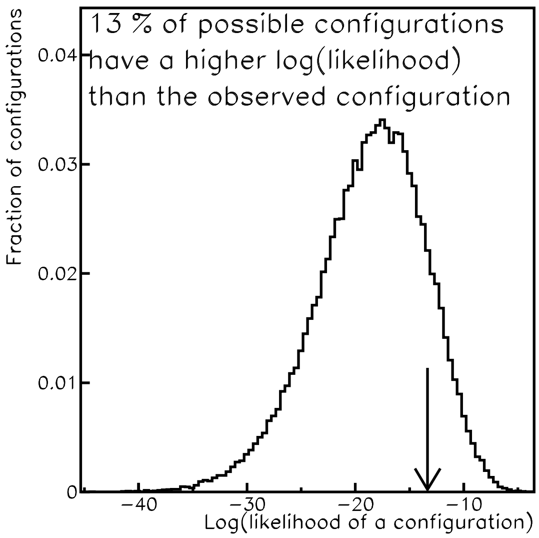

FIG. 5. The comparision of the log(Likelihood) for many "experiments" with four signal events with the log(Likelihood) of the charm meson decay mode configuration that is observed (shown by the arrow) in data.

National Science Foundation, the U.S. Department of Energy, and the Natural Sciences and Engineering Research Council of Canada.

REFERENCES

[1] R.M. Barnett *et al.* Review of Particle Physics, Phys. Rev **D54**, 1 (1996).
[2] D. M. Asner *et al.* (CLEO Collaboration), Phys. Rev. Lett. **79**, 799 (1997).
[3] R. Barate *et al.* (ALEPH Collaboration), CERN Preprint CERN-PPE/98-037 (1998).
[4] Y. Kubota *et al* (CLEO Collaboration), Nucl. Inst. Meth. **A320**, 66 (1992).
[5] R. Brun *et al.* GEANT3 Users Guide, CERN DD/EE/84-1 (1987).
[6] L. Gibbons, *et al.* (CLEO Collaboration), "The Inclusive Decays $B \to DX$ and $B \to D^*X$", Phys. Rev. **D56**, 3783 (1997).
[7] C.S. Jessop *et al.* (CLEO Collaboration), "Measurement of the Decay Amplitudes and Branching Fractions of $\mathrm{B} \to \mathrm{J}/\psi\mathrm{K}^*$ and $\mathrm{B} \to \mathrm{J}/\psi\mathrm{K}$ Decays", Phys. Rev. Lett. **79**, 4533 (1997).